Supporting Information

Trajectory Angle Determination in One Dimensional Single Molecule Tracking Data by Orthogonal Regression Analysis

Khanh Hoa Tran Ba, Thomas A. Everett, Takashi Ito and Daniel A. Higgins**

Department of Chemistry, Kansas State University, Manhattan, KS, 66506-0401

Additional details on sample preparation and characterization are provided. Included are the chemical structure of OPPDI (**Scheme S1**) and typical X-ray diffraction data obtained from the mesoporous films (**Figure S1**). Also provided is a detailed description of the method used to link fluorescent spots into trajectories. The wide-field fluorescence video from which Figure 1 is derived is given (**Video 1)**, along with representative images and videos obtained under linearly polarized excitation (**Figure S2**, **Videos 2-3**). The video used in Figure 2 is also provided (**Video 4**). Single molecule trajectory simulations are described and simulated data used in determining the error rate in assigning 1D-diffusing and 2D-diffusing/immobile populations is shown (**Figure S3)**. Data from a repeat analysis of the trajectory angle data (Figure 4, main text) using the trajectory variance ratio as an alternative means to distinguish 1D-diffusing and 2D-diffusing/immobile populations is presented (**Figure S4**). Representative trajectory angle distributions for simulated 1D and 2D-diffusing molecules are presented (**Figure S5**) along with the simulated videos (**Videos 5-6**). Finally, histograms showing the diffusion coefficients for the 1D-diffusing and 2D-diffusing/immobile populations found in Figure 1 are given (**Figure S6**).

Experimental Considerations

Sample Preparation

Sols for the preparation of surfactant-templated silica thin films were prepared as described previously.[1, 2] Briefly, these were obtained by mixing tetramethoxysilane (99%, TMOS, Aldrich), deionized water (HPLC grade, Acros), absolute ethanol (200 proof, HPLC grade, Sigma-Aldrich) and HCl (ACS grade, Fisher) in a small vial. After addition of the above components, the sol was stirred for 1 h and was then allowed to age for an additional 24 h at room temperature in a dessicator. Cetyltrimethylammonium bromide (CTAB, Aldrich) was then dissolved in the sol by vigorous stirring for 1 h. The final molar ratio in the sols was typically 1:49.1:0.01:12.3:0.2 for TMOS, ethanol, HCl, H_2O and CTAB, respectively. Dye-doped mesoporous silica films were prepared by adding an isopropanol solution of bis-N,N'-(octyloxypropyl)perylene-3,4,9,10-tetracarboxylic diimide (OPPDI) to a portion of the above sol to yield a total dye concentration of 2 nM. OPPDI was synthesized by following previously-described procedures;[3, 4] its structure is shown in Scheme S1.

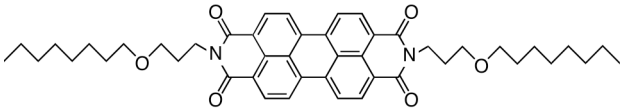

Scheme S1. Structure of bis-N,N'-(octyloxypropyl)perylene-3,4,9,10-tetracarboxylic diimide (OPPDI) used as the fluorescent tracer in single molecule tracking experiments.

Film deposition was accomplished by a method previously termed "vertical spin coating" in which the sample was spun along an axis parallel to the substrate plane.[5] In this procedure, ~ 100 µL of sol was spin cast (30s at 10,000 rpm) onto a plasma cleaned glass coverslip (Fisher Premium) immediately after addition of dye to the sol. The films were subsequently dried overnight at room temperature in a dessicator before use. The mean film thickness in samples

thus prepared was determined to be 180 ± 20 nm by spectroscopic ellipsometry (α-SE, J. A. Woollam). Surface profilometry measurements (XP-2, Ambios Technology) were used to confirm the film thickness obtained by ellipsometry and to quantify root-mean-square surface roughness, which was found to be 9 ± 3 nm. The latter value provides important confirmation that the films are continuous.

The presence of hexagonally-ordered cylindrical mesopores in the films was confirmed by X-ray diffraction.[1, 6] X-ray measurements were performed on a Bruker D8-Advance powder X-ray diffractometer using Cu Kα-radiation (40 KV, 40 mA) at 1.54 Å with a 0.05° step size and a 3 s step time. Representative X-ray diffraction data is shown in Figure S1.

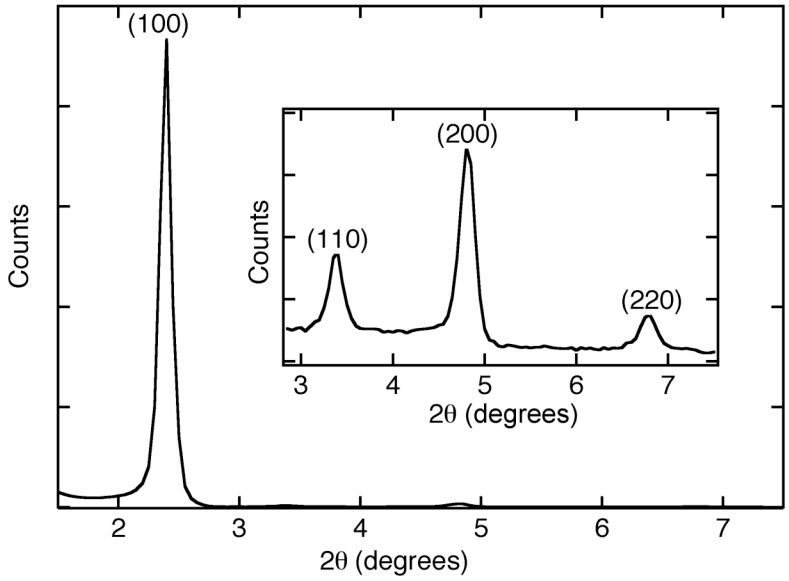

Figure S1. Typical X-Ray diffraction data from a surfactant-templated mesoporous silica film. The X-ray pattern is consistent with a hexagonal structure having characteristic (100) and (200) peaks at 2θ = 2.35° and 4.75°, respectively. Small intensity (110) and (220) peaks indicate that the sample also incorporates a small degree of 3D hexagonal or cubic symmetries. The inset depicts the (110), (200) and (220) peaks from the sample.

Instrumentation

All single-molecule studies were conducted on a wide-field fluorescence microscope. This system is built on an inverted epi-illumination microscope (Nikon Eclipse Ti), which was supported on a pneumatic vibration isolation table. Light from a blue diode laser (488 nm) was used to excite the dye molecules. Prior to incidence on the sample, the laser light was passed though appropriate band-pass filters and polarization optics. Both linear and circularly-polarized light were employed in separate experiments. Linearly polarized light was produced by use of an appropriate polarizer and 488 nm half-wave plate (Special Optics). Circularly polarized light was obtained by inserting a 488 nm quarter-wave plate (Special Optics) into the beam path, with its optical axis rotated 45^{o} from the incoming polarization. For uniform illumination of the sample, the laser light was also passed through a diffuser. It was subsequently reflected from a dichroic beamsplitter (505 nm cutoff) and into the back aperture of an oil immersion objective (Nikon Apo TIRF 100x, 1.49 N.A.). The incident laser power was maintained in the 0.5 – 1 mW range (estimated from measurements made just prior to the dichroic beamsplitter). An electronic shutter was used to control sample illumination. Fluorescence from the film was collected in reflection and was separated from the excitation light by passage back through the dichroic beamsplitter and appropriate bandpass (550 nm passband center wavelength, 40 nm width) and long-pass (515 nm cutoff) filters. A back-illuminated EM-CCD camera (Andor iXon DU-897) was used as the detector.

Wide-field movies were recorded as 100 frame videos with 0.33 s exposure times per frame. The image size was 512 pixels x 512 pixels, corresponding to an 87 μm x 87 μm (1 pixel = 0.17 μm) region in the sample. One dimensional diffusion in large ordered domains was only observed in previous studies after exposure of the films to high humidity environments.[7] Therefore, prior to the recording of videos, the samples were hydrated for 1 h at a relative humidity (RH) of ~70 % and/or imaged under a mixture of ethanol and water vapor. The same RH atmosphere was maintained throughout all experiments.

Trajectory Analysis

Automated Spot Detection and Linking in Trajectories

The tracking of single molecules across multiple video frames requires initial detection of individual molecules (i.e., as single fluorescent spots) and determination of their positions in each frame. The individual molecules appearing in the sequence of video frames must then be linked into trajectories. Molecule detection and position determination can be accomplished by any of a number of published methods.[8-10] Molecular position can often be determined to a precision well beyond the diffraction limit (i.e., ~λ/2), with localization precision as small at ~ 5-10 nm reported under relatively high, but common, signal-to-noise levels in single molecule tracking experiments.[7, 11-13] In the present work, molecule detection, validation and position determination were accomplished using methods reported by Sbalzarini and Koumoutsakos[8] and implemented in an ImageJ plugin.[14]

The linking of fluorescent spots in video frame sequences has been accomplished previously by manual[15] and semi-automated[16, 17] procedures, the former relying largely on human judgment. Manual linking was precluded in the present studies by the need to analyze large numbers of trajectories. Fully automated linking was instead employed and was accomplished by implementation of modified literature-based methods.[8] In these methods, a linear cost functional (Eqn. 14, Ref 8)[8] is defined and subsequently minimized to determine frame-to-frame associations of individual fluorescent spots. The cost, ϕ of linking spot j in frame t to spot k in frame t+1 was initially determined by:

$$\phi_{jk}(t,t+1) = \left(x_j(t) - x_k(t+1)\right)^2 + \left(y_j(t) - y_k(t+1)\right)^2 \quad \text{(S1)}$$

in which (x_j, y_j) represents the x, y position of spot j. The cost functional was evaluated globally, for all pairs of spots during initial spot linking.

After initial construction, the trajectories were subsequently refined by iteration through the spot linking process using a variant of the previous cost functional:[18]

$$\phi_{ijk}(t-1,t,t+1) = \left(x_i(t) - x_j(t+1)\right)^2 + \left(y_i(t) - y_j(t+1)\right)^2 + w\left(1 - \frac{\left(\left(x_i(t-1) - x_j(t)\right)\left(x_j(t) - x_k(t+1)\right) + \left(y_i(t-1) - y_j(t)\right)\left(y_j(t) - y_k(t+1)\right)\right)^2}{\left(\left(x_i(t-1) - x_j(t)\right)^2 + \left(y_i(t-1) - y_j(t)\right)^2\right)\left(\left(x_j(t) - x_k(t+1)\right)^2 + \left(y_j(t) - y_k(t+1)\right)^2\right)}\right) \quad \text{(S2)}$$

The new term in Eqn. S2 represents the quantity ($1-\cos^2\delta\theta$), where $\delta\theta$ is the change in direction of molecule motion required to link three spots in three consecutive frames, and w is a weighting factor, empirically set to 2 in the present implementation. Application of Eqn. S2 during the spot linking process effectively dissociates trajectories incorporating two or more 1D segments into separate 1D trajectories. The resulting 1D trajectory segments are used below to visualize and quantify trajectory orientation and order in local sample regions.

Results and Discussion

Observation of Single Molecule Motion

Video 1. One hundred frame video depicting single molecule motions in a surfactant templated mesoporous silica thin film. Fluorescence in this video was excited using circularly-polarized light.

The data depicted in Figure 1A were recorded under circularly-polarized excitation, allowing for efficient excitation and detection of all dye molecules oriented in the film plane. Videos recorded under linearly-polarized excitation provide additional information on the orientation of molecules diffusing through the mesopores.[7] Figures S2A,B depict representative frames from Videos 2 and 3 of identical sample regions recorded using orthogonal excitation polarizations. Figures S2C,D plot the trajectories determined from each video and show that trajectories exhibiting 1D motion along the vertical direction appear when the excitation light is

polarized along this direction. Likewise, trajectories oriented along the horizontal direction appear when the incident light is polarized along the horizontal direction. As the transition dipole associated with excitation of OPPDI by 488 nm light is known to be polarized along the molecular long axis (Scheme S1),[19, 20] it is concluded the dye diffuses in an aligned state, with its long axis oriented parallel to the local channel axis. Similar conclusions have been drawn for diffusion of terylene diimides in related materials.[7]

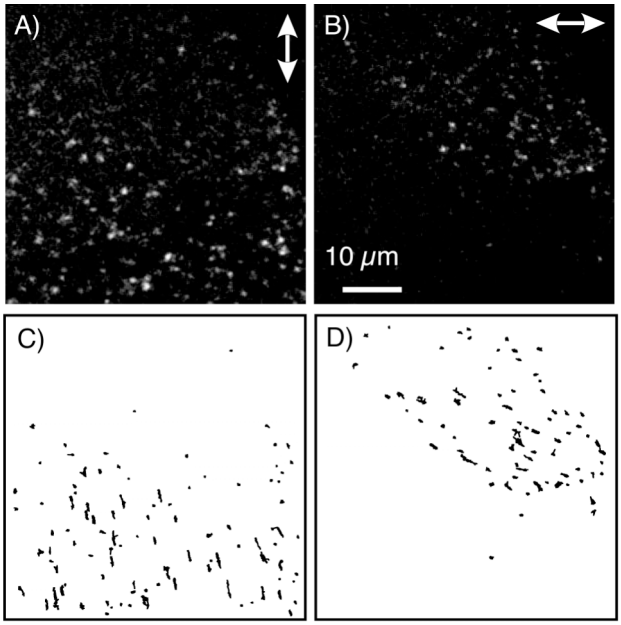

Figure S2. A) and B) Representative frames of two separate 100 frame videos recorded from identical regions of a surfactant-templated mesoporous silica thin film. Fluorescence in these videos was excited using linearly polarized light, as designated by the appended white arrows. The videos are provided as Videos 2, 3. C) and D) Trajectories depicting the motions of the individual molecules in these videos. To enhance trajectory visibility, only those ≥ 10 frames in length are shown.

Video 2. One hundred frame video recorded from the identical region of a surfactant templated mesoporous silica thin film as Video 3. Fluorescence in these videos was excited using linearly polarized light, as designated by the white arrow in Figure S2A.

Video 3. One hundred frame video recorded from the identical region of a surfactant templated mesoporous silica thin film as Video 2. Fluorescence in these videos was excited using linearly polarized light, as designated by the white arrow in Figure S2B.

Video 4. One hundred frame video depicting single molecule motions in a surfactant templated mesoporous silica thin film. Fluorescence in this video was excited using circularly-polarized light.

Analysis of Trajectory Angles

Simulated wide field videos were obtained using custom simulation software written in the National Instruments LabView programming environment. In these simulations, molecules were first positioned at random throughout the simulated region. Molecular diffusion was simulated by selecting the frame-to-frame step size (and direction) for each molecule from a Gaussian distribution (in each dimension) having a variance of $2Dt$. Here, t is the frame time (0.33 s) and D the diffusion coefficient of the mobile species. Each video was 100 frames in length. Videos simulating both 1D and 2D diffusion incorporated 100 molecules in a 43.5 μm x 43.5 μm region. Each molecule was assigned a lifetime (i.e., time to photobleaching), generated at random from an exponential distribution having a mean lifetime of 13 s. To maintain a constant concentration of molecules in the simulated region, bleaching of one molecule triggered positioning of a new molecule at a random position. For 2D simulations, each molecule was assigned a diffusion coefficient of 3×10^{-12} cm^2/s to properly model the experimental data, which depicts very slow diffusion for this population (see Figure S6). Simulations of 1D molecular motion employed a

diffusion coefficient of $3x10^{-10}$ cm^2/s. The signal-to-noise ratio in the images was set to a value that closely approximated the experimental data. The simulated videos were analyzed in a manner identical to analysis of the experimental videos. Figure S3A depicts the distribution of trajectory angle errors obtained from 3 separate simulations of 2D-diffusing species. Appended to Figure S3A is a Log Normal fit to the data. This fit was used to determine the probability that 2D-diffusing molecules would be erroneously classified as 1D-diffusing. As described in the main text, trajectories having $\sigma_\theta < 3.35^o$ were classified as 1D-diffusing molecules, while those with $\sigma_\theta \geq 3.35°$ were classified as 2D-diffusing or immobile molecules. The area under the Log Normal fit below the threshold was 5.5% of the total area under the curve, indicating a 5.5% error rate at which 2D trajectories will accidentally be classified as 1D trajectories. Figure S3B depicts the distribution of the trajectory variance ratio from the same data set and its fit to a Log Normal function. An error rate of 5.5% occurs in this data at a variance ratio of 0.197, the threshold value used for separation of 1D and 2D trajectories based on variance ratio data.

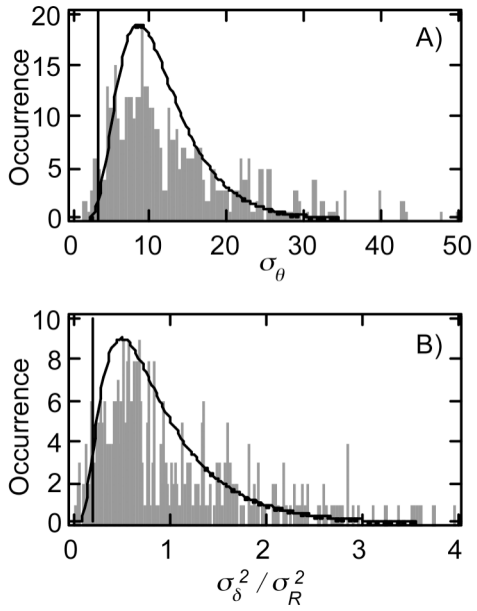

Figure S3 . A) Distribution of trajectory angle error (σ_θ) derived from 3 simulated movies. Also shown is a Log Normal fit to the data (solid line). The latter was used to determine the error rate for a threshold of $\sigma_\theta = 3.35°$. B) Distribution of the trajectory variance ratio and Log Normal fit (solid line). The variance ratio threshold for distinguishing 1D from 2D-diffusing and immobile molecules was determined to be 0.197.

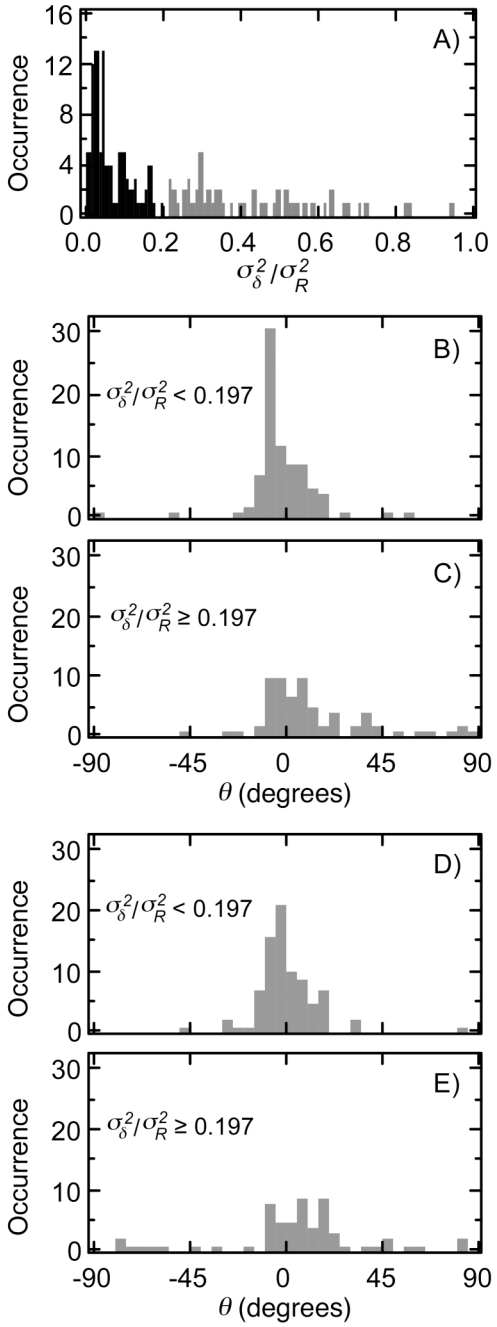

Figure S4. A) Distribution of $\sigma_\delta^2/\sigma_R^2$ values derived from the data in Video 1. Variance ratios for 1D-diffusing and 2D/immobile populations are shown in black and gray, respectively. The data were divided into two populations using a threshold of $\sigma_\delta^2/\sigma_R^2$ = 0.197, as described in the main text and in the simulation results above. B), C) Distributions of trajectory angles for 1D-diffusing species ($\sigma_\delta^2/\sigma_R^2$ < 0.197) and for

2D-diffusing/immobile species ($\sigma_\delta^2/\sigma_R^2 \geq 0.197$), respectively. D), E) Corresponding distributions of trajectory angles determined from the average step angle for each trajectory. Only data for trajectories ≥ 25 frames in length are shown. These results are nearly identical to those shown in Figure 4 (main text).

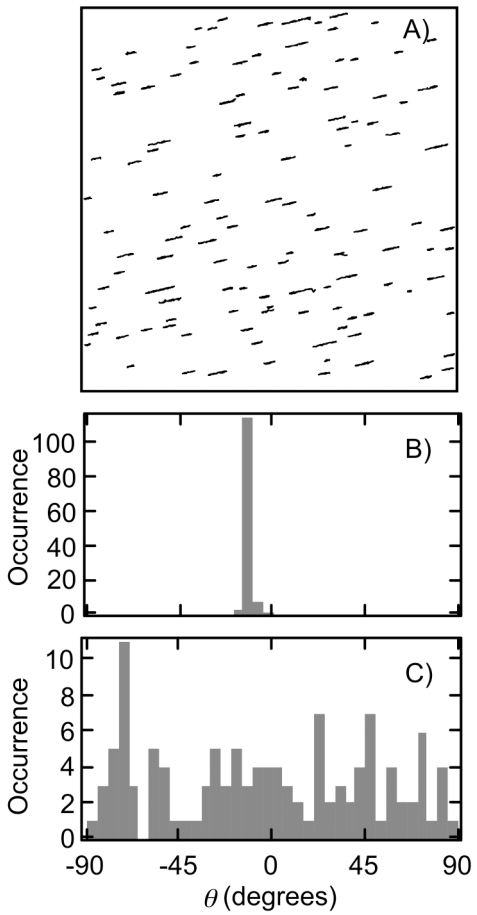

Figure S5. A) Trajectories from simulations of 1D-diffusing molecules. B), C) Distributions of trajectory angles for simulated 1D-diffusing and simulated 2D-diffuing species, respectively. In A), all trajectories were assigned an angle of -12.5°. All molecules were assigned diffusion coefficients of D = 3.0x10^{-10} cm^2/s. All simulation conditions (image area, dye concentration, bleaching rate, signal-to-noise ratio, etc.)

were set to approximate those of the experimental data described in the main text. Videos from which these data were obtained are provided as Videos 5 and 6.

Video 5. Simulated one hundred frame video depicting 1D-diffusing species. All molecules were assigned diffusion coefficients of $D = 3.0\text{x}10^{-10}$ cm^2/s.

Video 6. Simulated one hundred frame video depicting 2D-diffusing species. All molecules were assigned diffusion coefficients of $D = 3.0\text{x}10^{-10}$ cm^2/s.

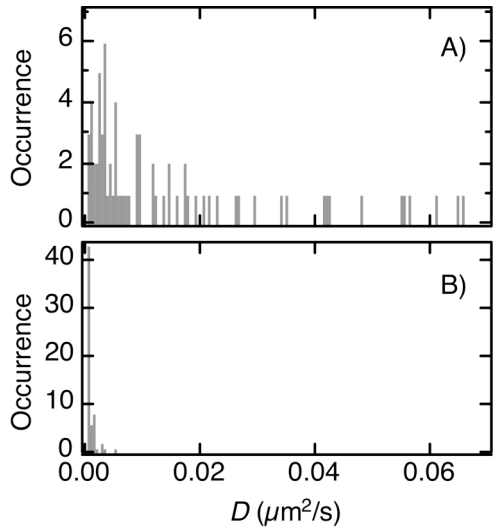

Figure S6. Histograms depicting the diffusion coefficients obtained from mean square displacement measurements along individual trajectories for A) $\sigma_\theta < 3.35°$ (1D-diffusing) and B) $\sigma_\theta \geq 3.35°$ (2D-diffusing/immobile) populations (data from Video 1).

References

1 Y. Fu, F. Ye, W. G. Sanders, M. M. Collinson and D. A. Higgins, *J. Phys. Chem. B*, 2006, **110**, 9164-9170.

2 F. Ye, D. A. Higgins and M. M. Collinson, *J. Phys. Chem. C*, 2007, **111**, 6772-6780.

3 T. A. Everett, A. A. Twite, A. Xie, S. K. Battina, D. H. Hua and D. A. Higgins, *Chem. Mater.*, 2006, **18**, 5937-5943.

4 J. J. Lange, C. T. Culbertson and D. A. Higgins, *Anal. Chem.*, 2008, **80**, 9726-9734.

5 K. Misawa, H. Ono, K. Minoshima and T. Kobayashi, *Appl. Phys. Lett.*, 1993, **63**, 577-579.

6 M. Klotz, P.-A. Albouy, A. Ayral, C. Menager, D. Grosso, A. Van der Lee, V. Cabuil, F. Babonneau and C. Guizard, *Chem. Mater.*, 2000, **12**, 1721-1728.

7 C. Jung, J. Kirstein, B. Platschek, T. Bein, M. Budde, I. Frank, K. Muellen, J. Michaelis and C. Braeuchle, *J. Am. Chem. Soc.*, 2008, **130**, 1638-1648.

8 I. F. Sbalzarini and P. Koumoutsakos, *J. Struct. Biol.*, 2005, **151**, 182-195.

9 A. Serge, N. Bertaux, H. Rigneault and D. Marguet, *Nature Methods*, 2008, **5**, 687-694.

10 K. Claytor, S. Khatua, J. M. Guerrero, A. Tcherniak, J. M. Tour and S. Link, *J. Chem. Phys.*, 2009, **130**, 164710.

11 N. Bobroff, *Rev. Sci. Instrum.*, 1986, **57**, 1152-1157.

12 T. Schmidt, G. J. Schutz, W. Baumgartner, H. J. Gruber and H. Schindler, *Proc. Natl. Acad. Sci.* , 1996, **93**, 2926-2929.

13 R. E. Thompson, D. R. Larson and W. W. Webb, *Biophys. J.*, 2002, **82**, 2775-2783.

14 G. Levy, Particle Tracker, 2009, http://rsb.info.nih.gov/ij/.

15 Y. Hou and D. A. Higgins, *J. Phys. Chem. B*, 2002, **106**, 10306-10315.

16 C. Seebacher, C. Hellriegel, F.-W. Deeg, C. Braeuchle, S. Altmaier, P. Behrens and K. Muellen, *J. Phys. Chem. B*, 2002, **106**, 5591-5595.

17 C. Hellriegel, J. Kirstein, C. Braeuchle, V. Latour, T. Pigot, R. Olivier, S. Lacombe, R. Brown, V. Guieu, C. Payrastre, A. Izquierdo and P. Mocho, *J. Phys. Chem. B*, 2004, **108**, 14699-14709.

18 D. Chetverikov and J. Verestoy, *Computing*, 1999, **62**, 321-338.

19 P. M. Kazmaier and R. Hoffmann, *J. Am. Chem. Soc.*, 1994, **116**, 9684-9691.

20 M. Adachi, Y. Murata and S. Nakamura, *J. Phys. Chem.*, 1995, **99**, 14240-14246.